XIX International Conference on Water Resources
CMWR 2012
University of Illinois at Urbana-Champaign
June 17-22,2012

DIRECT SIMULATIONS OF INTERFACE DYNAMICS: LINKING CAPILLARY PRESSURE, INTERFACIAL AREA AND SURFACE ENERGY

Andrea Ferrari*, Ivan Lunati

Institute of Geophysics, University of Lausanne, Amphipole - UNIL Sorge, 1015 Lausanne, Switzerland.
*e-mail: andrea.ferrari@unil.ch

Key words: Pore-Scale modeling, multiphase flow in porous media, Navier-Stokes simulations, Volume Of Fluid (VOF) method.

Summary. We perform direct numerical simulations of drainage by solving Navier-Stokes equations in the pore space and employing the Volume Of Fluid (VOF) method to track the evolution of the fluid-fluid interface. After demonstrating that the method is able to deal with large viscosity contrasts and to model the transition from stable flow to viscous fingering, we focus on the definition of macroscopic capillary pressure. When the fluids are at rest, the difference between inlet and outlet pressures and the difference between the intrinsic phase average pressure coincide with the capillary pressure. However, when the fluids are in motion these quantities are dominated by viscous forces. In this case, only a definition based on the variation of the interfacial energy provides an accurate measure of the macroscopic capillary pressure and allows separating the viscous from the capillary pressure components.

1 INTRODUCTION

Numerical simulations provide valuable tools to investigate the dynamics of a front invading a porous medium. Pore-network models (e.g.,[1, 2, 3]) have been widely employed to investigate two-phase flow in porous media due to their limited computational costs that allow considering a large number of pores. However, pore-network models are based on several modeling assumptions which limit their validity for benchmarking conceptual and theoretical models of flow at larger scales. At this end, methods based on conservation principles and resolving the dynamics in the pore are required (see [4] for a comprehensive review and discussion of the different methods).

Here, we focus on the Volume of Fluid (VOF) method [5], which can accurately describe the dynamics of the interfaces between two immiscible fluids and can naturally account for the contact angle [5, 6, 7, 8]. After a brief description of the method, we perform a set of drainage simulations to investigate several definitions of macroscopic capillary pressure during the transition from stable to unstable displacement.

2 GOVERNING EQUATIONS AND VOF METHOD

The motion of two incompressible, immiscible fluids at pore scale is governed by the Navier-Stokes equations for mass and momentum conservation, i.e.

$$\nabla \cdot \boldsymbol{u} = 0, \tag{1}$$

$$\frac{\partial \rho \boldsymbol{u}}{\partial t} + \nabla \cdot (\rho \boldsymbol{u}\boldsymbol{u}) = -\nabla p + \nabla \cdot (\mu \boldsymbol{S}) + \boldsymbol{f}_{sa}, \tag{2}$$

where $\boldsymbol{u}$ is the velocity, ρ the density, p the pressure, μ the viscosity, $\boldsymbol{S} = \nabla \boldsymbol{v} + \nabla \boldsymbol{v}^T$ the rate of strain, and $\boldsymbol{f}_{sa}$ accounts for the surface tension acting at the interface between the two fluids. (Gravity is neglected).

In the Eq. 2 viscosity and density vary in space depending on the fluid present. Here we use the Volume of Fluid method (VOF [5]) and describe the distribution of the two fluids by the fluid fraction or color function, F, which is equal to 1 in the non-wetting fluid and 0 in the wetting fluid. The color function evolves in time according to a simple advection equation,

$$\frac{\partial F}{\partial t} + \nabla \cdot (F \boldsymbol{u}) = 0, \tag{3}$$

where the velocity is obtained by solving the Navier-Stokes equations.

When Eqs. 1–3 are discretized on a grid and solved numerically, the color function represents the volumetric fraction of the non-wetting fluid in the cell. At the interface between the two fluids, the color function assumes values between 0 and 1, and density and viscosity are computed as weighted averages of the properties of the two phases, i.e., $\rho = F\rho_{nw} + (1-F)\rho_w$ and $\mu = F\mu_{nw} + (1-F)\mu_w$.

The surface force acting at the fluid-fluid interface is described by the Continuum Surface Force method (CSF [9]), which models the surface force as a body force of the form

$$\boldsymbol{f}_{sa} \approx \boldsymbol{f}_{sv} = \sigma \kappa \nabla F, \tag{4}$$

where σ is the surface tension,

$$\kappa = -\nabla \cdot \boldsymbol{n} = \nabla \cdot \left(\frac{\nabla F}{|\nabla F|} \right), \tag{5}$$

the curvature and $\boldsymbol{n}$ the normal to the surface, which is computed from the color function as indicated above. Note that $\boldsymbol{f}_{sv}$ acts only in presence of color-function gradients (thus, in the interface region where $0 < F < 1$) and converges to the exact surface force, $\boldsymbol{f}_{sa} = \sigma \kappa \delta_S \boldsymbol{n}$, when the thickness of the transition region tends to zero (δ_S is the Dirac function indicating the surface).

The interaction between the fluids and the solid is described by the contact angle, which is easily included in the CSF-VOF method as a boundary condition for the surface normal vector at the solid wall [5, 6, 7, 9]. The numerical simulations presented in the rest of the paper are performed with a modified version of OpenFoam [12].

Property	**SQUARES**	**CIRCLES**
Domain dimensions	88×114 mm^2	88×114 mm^2
Mean distance between obstacles (a)	400 μm	400 μm
Number of obstacles	9.856	10.028
Number of computational cells	2.663.936	2.767.077
Permeability (k)	6.85 10^{-9} m^2	9.5 10^{-9} m^2
Porosity (ϕ)	64%	68%

Table 1: Properties of the two geometries used in the simulations

3 NUMERICAL SIMULATIONS OF DRAINAGE

Drainage is simulated in two geometries that idealize the porous medium as a two-dimensional horizontal domain that incorporates a set of obstacles. In first geometry, the obstacles consist of identical squares which are placed at a random distance from the nodes of a regular lattice; in the second geometry, the obstacles are circles placed at random positions. The properties of the two geometries are summarized in Table 1.

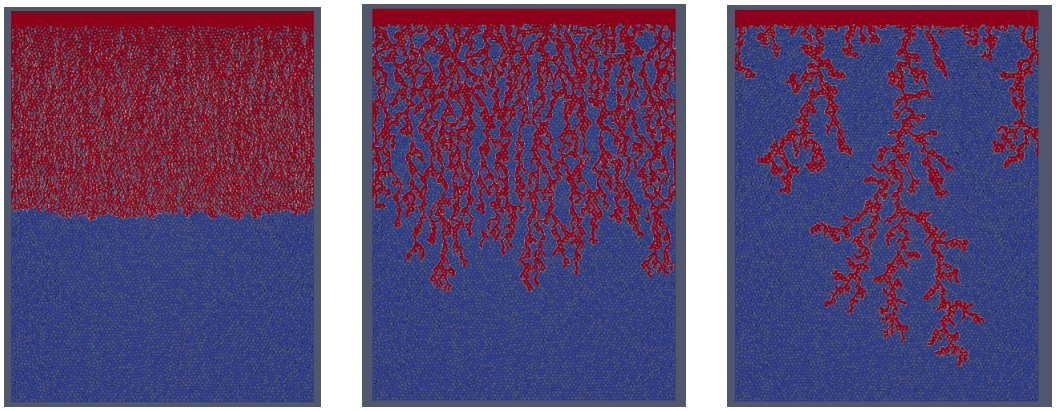

(a) $M = 3$ (b) $M = 0.2$ (c) $M = 4\ 10^{-4}$

Figure 1: Transition from stable to unstable displacement for the geometry with circular obstacles at Ca $= 0.13$. The VOF color function is shown for three different viscosity ratio: a) $M = 3$, the invading phase saturation is $S_{nw} = 0.49$, b) $M = 0.2$, the invading phase saturation is $S_{nw} = 0.40$ and c) $M = 4\ 10^{-4}$, the invading phase saturation is $S_{nw} = 0.22$

For the injection rates considered here, the flow is characterized by two dimensionless numbers

$$\mathrm{Ca} = \frac{U\mu_w a^2}{\sigma k} \qquad \text{and} \qquad \mathrm{M} = \frac{\mu_{nw}}{\mu_w}, \tag{6}$$

where U the injection velocity (constant at the inlet), a the mean distance between the obstacles, k the intrinsic permability, σ the surface tension, and μ_w, resp. μ_{nw}, the viscosity of the wetting, resp. non-wetting, fluid (fluid properties are summarized in

Property	**Value**	**Unit**
Contact angle (θ)	30	$deg.$
Interfacial tension (σ)	0.064	$kg\ s^{-2}$
Viscosity of the wetting phase (μ_w)	0.05	$kg\ m^{-1}\ s^{-1}$
Viscosity ratio ($M = \frac{\mu_{nw}}{\mu_w}$)	$4\ 10^{-04}$, 0.02, 0.2, 3.3	-

Table 2: Fluid properties

Table 2). The capillary number, Ca, represents the relative effects of viscous versus capillary forces, whereas M is the viscosity ratio. (Note that inertia can be neglected as the Reynolds number is $\mathrm{Re} = \frac{\rho_w U a}{\mu_w} < 10^{-1}$ in all simulations).

In Fig 1 the fluid distribution is shown for three simulations with Ca = 0.13 and different viscosity ratios, i.e., $M = 4\ 10^{-4}$, $M = 0.2$ and $M = 3$. The transition from stable to unstable displacement is clearly visible: in case of favorable viscosity ratio ($M > 1$) the front is compact and fewer pores remain filled by the wetting phase behind the front. In case of unfavorable viscosity ratio ($M < 1$), the flow undergoes a transition to viscous fingering ($M = 4\ 10^{-4}$). These results are in agreement with experimental observations in two-dimensional porous media (see, e.g., [10]), and demonstrate the capability of the VOF to model the interplay between capillary and viscous forces.

The difference between the intrinsic phase average pressures,

$$\Delta p_{\mathrm{pa}} = \langle p \rangle_{nw} - \langle p \rangle_w = \frac{\langle pF \rangle}{\langle F \rangle} - \frac{\langle p(1-F) \rangle}{\langle (1-F) \rangle}, \tag{7}$$

is shown in Fig 2 as a function of the average saturation of the non-wetting fluid,

$$S_{nw} = \langle F \rangle = \frac{1}{V} \int_V F \ dv, \tag{8}$$

where the angle brackets denote the average over the volume accessible to the flow, V.

Fig 2a shows the results at Ca = 0.13 and different viscosity ratios ($M = 4\ 10^{-4}$, $2\ 10^{-2}$, 0.2, and 3) for the geometry with circular obstacles. For unfavorable viscosity ratios, breakthrough happens at earlier time and the pressure difference decreases with the saturation due to the lower viscosity of the injected fluid. In the favorable case, the pressure difference increases at lower saturation and decreases at larger saturations.

Fig 2b shows the results of drainage simulation in the geometry with square obstacles at $M = 4\ 10^{-4}$ and different capillary numbers. Larger capillary numbers result in a larger pressure difference due to larger viscous effects. After a rapid build up due to the effects of the entry pressure when the invading front reaches the porous medium, the pressure difference steadily decreases with drainage. This is due to the negligible viscosity of the invading fluid with respect to the viscosity of the defending fluid, which reduces the overall viscous dissipation in the porous medium. A similar behavior has been experimentally observed during drainage of glass-bead monolayers [11].

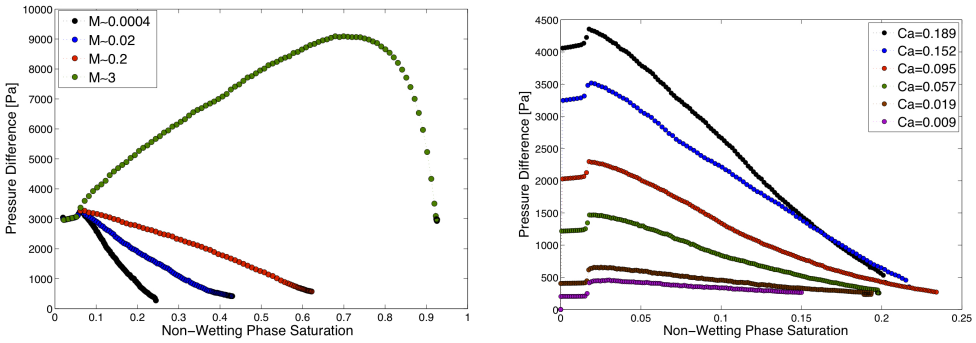

(a) (b)

Figure 2: Difference between the intrinsic phase average pressures, Eq. 7 as a function of the saturation of the non-wetting fluid. (a) Simulations at Ca = 0.13 for different M in the geometry with cyrcular obstacles; (b) simulations at $M = 4\ 10^{-4}$ for different Ca in the geometry with square obstacles.

4 CAPILLARY PRESSURE AND SURFACE ENERGY

As can be observed in Fig 2, the difference between the intrinsic phase average pressures is strongly affected by viscous effects and cannot be taken as an accurate estimate of the macroscopic capillary pressure when the fluids are moving. In this section we consider a definition that relates the capillary pressure to its physical origin: the surface energies.

The infinitesimal increment of the Helmholtz free energy is

$$dF = -p_{nw}dV_{nw} - p_w dV_w + \sum_i^3 \sigma_i dA_i \tag{9}$$

where the sum is taken over the three surfaces: the dry solid (with surface tension σ_{ns} and area increment dA_{ns}); the wet solid (σ_{ws} and dA_{ws}); and the fluid-fluid interface (σ and dA). At equilibrium we have $dF = 0$, and by observing that $dV_w = -dV_{nw}$ and $dA_{ws} = -dA_{ns}$ we obtain

$$p_c = p_{nw} - p_w = \sum_i^3 \sigma_i \frac{dA_i}{dV_{nw}} = \sigma \left(\frac{dA}{dV_{nw}} + \frac{dA_{ws}}{dV_{nw}} \cos\theta \right), \tag{10}$$

where we have used Young's law, $\sigma_{ns} - \sigma_{ws} = \sigma \cos\theta$.

When the fluids are at rest their pressure is constant and the difference between inlet and outlet pressure, Δp_{io}, the difference between the intrinsic phase average pressures, Δp_{pa} in Eq. 7, and p_c defined in Eq. 10 give the correct capillary pressure. To compare these quantities when the fluids are in motion, we simulate a quasi-static drainage experiment: the injection of a small amount of fluid at constant velocity is followed by a relaxation stage during which injection is stopped and the menisci move until they reach an equilibrium position.

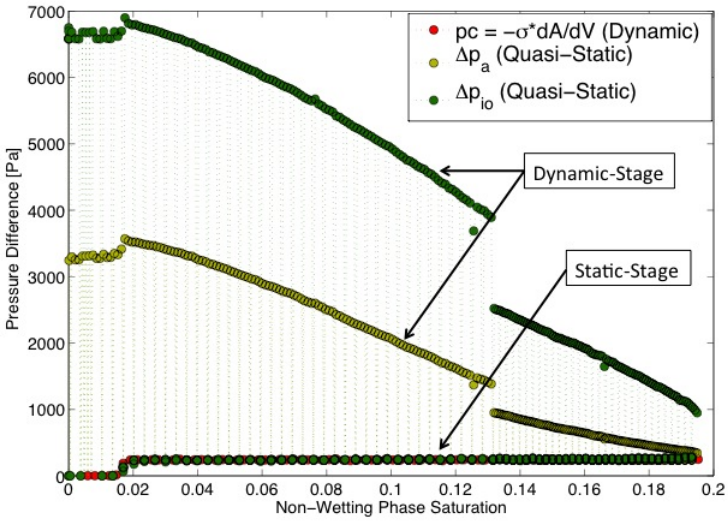

Figure 3: Comparison among the difference between the intrinsic phase-average pressure, $\Delta p_{\rm pa}$, in a quasi-static drainage experiment (yellow); the difference between inlet and outlet pressure, $\Delta p_{\rm io}$, in a quasi-static drainage experiment (green); and the capillary pressure calculated with Eq. 10 in a dynamic drainage experiment (red). When the injection stops, $\Delta p_{\rm pa}$ and $\Delta p_{\rm io}$ relax towards the capillary pressure defined by Eq. 10.

In Fig 3 the inlet-outlet pressure difference and intrinsic phase-pressure difference, Eq. 7, during the quasi-static drainage simulation are compared with the capillary pressure computed from Eq. 10 for a dynamic simulation with the same capillary number and viscosity ratio. When injection stops, the inlet-outlet pressure difference and the intrinsic phase-pressure difference relax towards the the static capillary pressure. The pressure jump at saturation $S_{nw} = 0.13$ corresponds to a change in the injection velocity, which reduces the capillary number from $\mathrm{Ca} = 0.15$ to $\mathrm{Ca} = 0.095$. Note that the pressure difference calculated from Eq. (10) under dynamic conditions coincides with the pressure difference at the equilibrium in quasi-static experiment. In Fig 4 the capillary pressure calculated from Eq. 10 is plotted as a function of the non-wetting phase saturation for the drainage simulations presented in the previous section. By comparison with Fig 2 it is evident that the definition relying on the variation of the surface energy is not sensitively affected by viscous forces.

5 CONCLUSIONS

The VOF method is able to deal with large viscosity contrast and to model the transition from stable flow to viscous fingering. Being based on conservation principles and on a rigorous physics that allows an explicit description of meniscus and contact-line dynamics

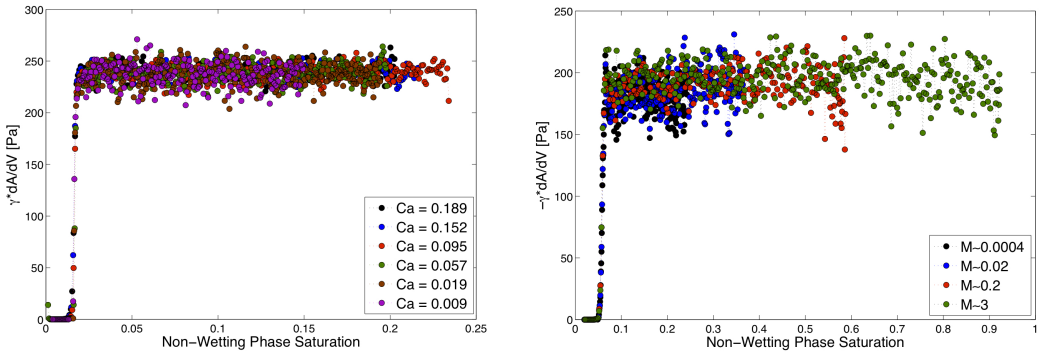

(a) (b)

Figure 4: Capillary pressure, based on (10). (a) simulations at Ca = 0.13 for different M in the geometry with cyrcular obstacles; (b) simulations at $M = 4\ 10^{-4}$ for different Ca in the geometry with square obstacles..

(at least within the accuracy limit set by the numerical discretization), the method offer a valuable tool to benchmark conceptual and theoretical models.

Here, we have used the VOF method to compare three different definitions of macroscopic capillary pressure that are equivalent when the fluids are at rest. However, when the fluids are in motion the difference between inlet and outlet pressure and the difference between the intrinsic phase average pressure are strongly dominated by viscous forces. In this case, only a definition based on the variation of the interfacial energy provides an accurate estimate of the macroscopic capillary pressure and allows separating viscous and capillary contributions.

For the numerical tests considered here, this definition of capillary pressure does not sensitively depend on the viscosity ratio and the capillary number. Although this is consistent with the idea that capillary pressure is a property of the fluid-solid system [3], this is likely due to the relatively small variability of the pore size in the geometries that we have considered and to the consequently flat capillary pressure-saturation curve. This issue needs to be further addressed in future works.

Acknowledgments

We thank Jan Ludvig Vinningland for providing the geometry consisting of circular obtascles. This project is supported by the Swiss National Science Foundation Grant No. FNS PP00P2_123419/1.

REFERENCES

[1] Fatt, I. [1956] The network model of porous media, Pet. Trans. AIME, 207:144181

[2] Blunt, M., and P. King [1990] Macroscopic parameters from simulation of pore scale flow, Phys. Rev. A, 42, 4780-4787

[3] V. J. Niasar, S. M. Hassanizadeh and H.K. Dahle [2010] Non-equilibrium effects in capillarity and interfacial area in two-phase flow: dynamic pore-network modelling. J. Fluid Mech. (2010), vol. 655, pp. 3871.

[4] Meakin, P., and A. M. Tartakovsky [2009] Modeling and simulation of pore-scale multiphase fluid flow and reactive transport in fractured and porous media, Rev. Geophys., 47, RG3002

[5] Hirt, C.W., and B.D. Nichols [1981] Volume of fluid (VOF) method for the dynamics of free boundaries. J. Comput. Phys., 39, 201-25.

[6] Huang, H., Meakin, P., Liu, M. [2005] Computer simulation of two-phase immiscible fluid motion in unsaturated complex fractures using a volume of fluid method. Water Resources Research, 41, 1-12.

[7] Lunati, I., and D. Or [2009] Gravity driven slug motion in capillary tubes, Physics of Fluids, 21(5), 052003

[8] Afkhami, S., S. Zaleski, M. Bussmann [2009] A mesh-dependent model for applying dynamic contact angles to VOF simulations J. Comput. Phys., 228, 5370-5389

[9] Brackbill, J. U., Kothe, D. B., Zemach, C. [1992] A continuum method for modeling surface tension. Journal of Computational Physics, 100, 335-354.

[10] R. Lenormand, E. Touboul, C. Zarcone [1988] Numerical models and experiments on immiscible displacements in porous media. J. Fluid. Mech. vol. 189, pp. 165-187

[11] G. Løvoll, M. Jankov, K. J. Maløy, R. Toussaint, J. Schmittbuhl, G. Schfer, Y. Méheust, [2010], Influence of Viscous Fingering on Dynamic SaturationPressure Curves in Porous Media. Transp Porous Med 86:305324

[12] OpenCFD Ltd., OpenFOAM User Guide, Version 2.0.0 Edition, 2011.